GLOBAL MODES CONSTITUTING THE SOLAR MAGNETIC CYCLE

II. *Phases, 'Geometrical Eigenmodes', and Coupling of Field Behaviour in Different Latitudes*

M. H. GOKHALE and J. JAVARAIAH

Indian Institute of Astrophysics, Bangalore 560 034, India

(Received 18 July, 1991; in revised form 21 October, 1991)

Abstract. We show that the axisymmetric odd degree SHF modes of 21.4-yr periodicity and degrees $l \leq 29$ in the solar magnetic field (as inferred from sunspot data during 1874–1976), are at least approximately stationary. Among the sine and cosine components of these SHF modes we find four groups, each defining the geometry of a *coherent global oscillation* characterized by a distinct power hump and its own level of variation. The first two of these 'geometrical eigenmodes' (viz., B_1 and B_2), define the large-scale structure of the butterfly diagrams. Remaining SHF modes define the orderliness of the field distribution even within the 'wings' of the 'butterflies' down to scales $l \approx 29$. These include the 'geometrical eigenmodes' B_3 and B_4, which are not present in simulated data sets in which the latitudes of the sunspot groups are randomly redistributed within the 'wings' of the 'butterflies'.

Superposition of B_1, B_2, B_3, and B_4 is *necessary and sufficient* to reproduce important observed properties of the latitude-time distribution of the real field, not only in the 'sunspot zone', but also in the middle ($35°-75°$) and the high ($\gtrsim 75°$) latitudes, with appropriate relative orders of magnitude and phases. Thus, B_1, B_2, B_3, and B_4 seem to represent really existing global oscillations in the Sun's internal magnetic field. The geometrical form of B_1 may also be the form of the 'forcing' oscillation.

1. Introduction

In Paper I (Gokhale *et al.*, 1992) we presented SHF spectra of the solar magnetic field, as inferred from the sunspot data during 1874–1976, and showed that in these spectra there is no evidence for the existence of any relation between the degree l and frequency ν of either the even degree or odd degree modes that have significant amplitudes. The 'power ridges' in the spectra suggested the presence of global oscillations in 'resonance' with some unidentified 'forcing oscillation' at frequency $1/21.4\ \mathrm{yr}^{-1}$ and its odd harmonics.

In this paper (Paper II) we use the information present in the computed phases of the SHF modes to identify four independent geometrical modes of coherent global oscillations – ('geometrical eigenmodes') – in the field, and show how these oscillations yield the observed global properties of the solar magnetic features.

In Section 2 we separate the stationary (or approximately stationary) and non-stationary modes in the main power ridge of the SHF spectrum and identify the four 'geometrical eigenmodes'. We also show that only the first two of these coherent oscillations can be found (the second one, or both, only partially) in the field defined by simulated data sets which simulate butterfly diagrams, but in which the latitudes of the sunspot groups are randomly redistributed within the wings of the butterflies. The eigenmodes B_3, B_4 are not present in the fields so defined.

Solar Physics **138:** 399–410, 1992.

In Section 3 we show how, one by one, the four 'geometrical eigenmodes' yield the various observed properties of the latitude-time distribution, of not only the sunspot activity in the lower latitudes, but also those of other solar magnetic features in *all* (viz., low, medium, and high) ranges of latitudes. Thus, these geometrical eigenmodes are not merely mathematical expressions of the latitude-time distribution of sunspot activity; they rather represent physically global oscillations actually existing in the Sun's magnetic field. The physical nature of these modes needs to be identified theoretically.

In Section 4 we compare our results for modes $l \leq 13$ with those obtained by Stenflo (1988) from the magnetogram data during 1960–1985, and give reasons for the minor differences.

In Section 5 we summarize the conclusions and discuss their significance. The physical nature of the oscillations $B_1 \ldots B_4$ is not known. However, it is noted once again that these oscillations have parities consistent with a torsional MHD oscillation of even parity if the zero-order field has dipole-like parity. It is also suggested that B_1 might be representing the geometrical form of the 'forcing' function.

2. Coherent Oscillations in the 'Main Power Ridge'

2.1. The Data and the Method of Analysis

The data used is the same as that used in Paper I, viz., Greenwich photoheliographic data for sunspot groups during 1874–1976 as recorded on a computer tape. (The tape was provided by H. Balthasar.) The method of analysis and the relevant formulae also are described in Paper I.

2.2. Variations in the Relative Phases of Modes in the 'Main Power Ridge'

In Paper I it was seen that in the SHF spectrum for the odd degree axisymmetric modes in the Sun's magnetic field inferred from sunspot data, the only outstanding features are the 'main power ridge' along $\nu = \nu_* = 1/21.4\ \mathrm{yr}^{-1}$ and subsidiary ridges along $\nu = n\nu_*$ for odd integral values of n. Following the procedure outlined in that paper, we determined the phases φ_l of the modes $l = 1$–35 in the 'main power ridge' during the eighty two intervals (during 1874–1976) each of 22 yr length and displaced by one year relative to the previous interval. As expected from the earlier somewhat cruder analysis (Gokhale *et al.*, 1990), the relative phases $\delta_l\,(= \varphi_l - \varphi_5)$ are approximately constant. For quantitative comparison of their constancy, we give in Table I the mean values (δ_l) and the standard deviations $(\Delta\delta_l)$ of δ_l for the field inferred from the real data set ('R') and also for fields derived from the two simulated data sets 'SI' and 'SII' described in Paper I. For clarity we re-state here that in 'SI' and 'SII' the time epochs of the sunspot groups were kept the same as those in the real data; but the latitudes of sunspot groups during each year, in each wing of the butterfly diagram, were redistributed randomly. In 'SI' the redistributions were made with Gaussian probability distributions with the means and standard deviations the same as in the real data. In 'SII' they were made

TABLE I

Mean values $\bar{\delta}_l$ and standard deviations $\Delta\delta_l$ of the relative phases δ_l ($= \varphi_l - \varphi_5$) of the odd degree modes of frequency 1/21.4 yr^{-1}, in the magnetic field inferred from real data set *R* and the simulated data sets SI and SII

l	*R*		SI		SII	
	$\bar{\delta}_l$	$\Delta\delta_l$	$\bar{\delta}_l$	$\Delta\delta_l$	$\bar{\delta}_l$	$\Delta\delta_l$
1	7.7°	1.4°	9.5°	4.3°	7.9°	1.57°
3	−174.5°	1.0°	−173.5°	3.2°	−174.7°	1.12°
5	0.0°	0.0°	0.0°	0.0°	0.0°	8.0°
7	170.4°	2.1°	167.4°	8.6°	169.3°	2.8°
9	−27.3°	6.0°	−30.5°	21.8°	−32.3°	10.0°
11	123.0°	10.3°	139.6°	27.9°	112.9°	16.9°
13	93.2°	9.6°	−35.8°	44.7°	−99.8°	11.5°
15	55.4°	9.1°	–	⩾30.0°	75.5°	31.9°
17	−155.5°	10.6°	–	–	−87.3°	77.4°
19	−9.6°	14.5°	–	–	–	⩾30.0°
21	142.3°	23.1°	–	–	–	–
23	−49.2°	32.7°	–	–	–	–
25	132.2°	35.2°	–	–	–	–
27	−10.5°	25.0°	–	–	–	–
29	190.9°	27.5°	–	–	–	–
31	−4.1°	70.4°	–	–	–	–
33	147.1°	97.6°	–	–	–	–
35	92.0°	77.9°	–	–	–	–

with uniform probability over the entire widths of the respective wings defined by the maximum and the minimum latitudes. In each simulation the data from the old cycles and the new cycles, during the overlaps of successive cycles, were treated separately.

The data samples during the successive 22-yr intervals are not statistically independent (since they overlap) and, hence, it may be thought that the r.m.s. variations should have been computed from a set of four or five non-overlapping intervals during 1874–1976. However, the mean values and the r.m.s. variations computed from the 82 intervals are equivalent to those computed from non-overlapping intervals with uniform weighting in time. Moreover, we have verified that the r.m.s. variations computed from non-overlapping intervals are actually smaller than those from the eighty-two intervals.

2.3. The stationary, approximately stationary, and non-stationary modes

From Table I we see that for each data set, the modes in the main ridge fall automatically into three categories:

(1) Stationary Modes: viz., modes with constant phases ($\Delta\delta_l \lesssim 15°$),

(2) Approximately Stationary Modes: viz., modes with approximately constant phases ($\Delta\delta_l \lesssim 30°$) and

(3) Non-Stationary Modes: viz., modes with large phase variations ($\Delta\delta_l \gg 30°$).

In Table II we list the modes of each category in the data sets *R*, SI, and SII.

TABLE II

List of modes of each category in the three data sets

Category	R (real data)	SI (gaussian)	SII (box)
$\Delta\delta_l \leq 15°$	l = 1–19	l = 1–7	l = 1–13
$\Delta\delta_l \leq 30°$	l = 21–29	l = 9–11	l = 15
$\Delta\delta_l \gg 30°$	$l \geq 31$	$l \geq 13$	$l \geq 17$

2.4. Presence of four modes of 'coherent global oscillations'

Using the complex amplitudes A_l (determined in Paper I) and relative phases δ_l we have computed the mean relative real amplitudes a_l ($= A_l \cos\delta_l$) and b_l ($= A_l \sin\delta_l$) of the sine and cosine (temporal) phases of the stationary and approximately stationary modes in the field inferred from the real data ('R') and that inferred from the simulated data set 'SII' (the set that simulates the real data more closely: cf. Paper I). These are given in Table III. In the same table, we also give the r.m.s. variations Δa_l and Δb_l of a_l and b_l. It can be seen that in each phase, there are groups of terms characterized by a range of l in which the respective 'phase-amplitude', a_l or b_l, is maximum near the centre and falls off to the noise level (i.e., ≤ 0.04) at both ends. The signs of the successive

TABLE III

Mean values (a_l, b_l) and r.m.s. variations (Δa_l, Δb_l) of the amplitudes of the sine and cosine components, respectively, of the SHF modes of odd degrees and 21.4-yr periodicity in the magnetic field inferred from two data sets. Groups of a_l and b_l printed in bold (separated by mean values below – or nearly equal to – the level of variation together with the breaks in the alternation of the signs) represent independent coherent global oscillations

l	Real data set				Simulated data set 'SII'			
	a_l	Δa_l	b_l	Δb_l	a_l	Δa_l	b_l	Δb_l
1	**0.247**	0.014	0.033	0.008	**0.249**	0.038	0.035	0.019
3	**−0.718**	0.026	**−0.065**	0.014	**−0.724**	0.069	−0.067	0.036
5	**1.000**[a]	0.028	**0.000**[a]	–	**1.000**[a]	0.070	0.000[a]	–
7	**−0.945**	0.081	**0.157**	0.024	**−0.916**	0.249	**0.169**	0.061
9	**0.636**	0.112	**−0.318**	0.035	**0.568**	0.374	**−0.334**	0.087
11	**−0.264**	0.095	**0.390**	0.031	**−0.184**	0.311	**0.385**	0.098
13	0.017	0.056	**−0.345**	0.036	−0.042	0.117	**−0.298**	0.153
15	**0.152**	0.047	**0.219**	0.044	0.077	0.183	0.142	0.160
17	**−0.171**	0.052	**−0.081**	0.039				
19	**0.137**	0.045	−0.018	0.028				
21	**−0.097**	0.047	**0.064**	0.024				
23	**0.069**	0.057	**−0.066**	0.022				
25	**−0.061**	0.052	**0.044**	0.018				
27	**0.061**	0.035	−0.013	0.019				
29	**0.060**	0.037	0.010	0.024				
31	0.052	0.060	0.015	0.028				

[a] By virtue of definition

phase-amplitudes in each group are alternately positive and negative, and this rule breaks at the ends of the respective l-ranges. The levels of the r.m.s. variations Δa_l or Δb_l within each group are mutually similar, and different from those in the other groups.

It is clear that the field inferred from the real data contains four *independent* geometrical modes of *coherent global oscillations* defined by the following expressions:

$$B_1 = \left[\sum_{l=1}^{11} a_l P_l(\mu)\right] \sin(2\pi \nu_* t)\,, \qquad B_2 = \left[\sum_{l=3}^{17} b_l P_l(\mu)\right] \cos(2\pi \nu_* t)\,,$$
$$B_3 = \left[\sum_{l=15}^{29} a_l P_l(\mu)\right] \sin(2\pi \nu_* t)\,, \qquad B_4 = \left[\sum_{l=21}^{25} b_l P_l(\mu)\right] \cos(2\pi \nu_* t)\,. \tag{1}$$

Pending identification of the physical nature of these oscillation modes, we call them '*geometrical eigenmodes*'.

2.4.1. *Confirmation*

We have confirmed that the geometrical eigenmodes $B_1 .. B_4$ get defined by the same combinations of a_l and b_l terms even when the relative phases are defined with respect to $l = 1$ instead of $l = 5$.

2.5. Absence of B_3 and B_4 in simulated data sets

Since the simulated data sets 'SI' and 'SII' do not yield even approximately constant phases for modes beyond $l = 11$ and 15, respectively (see Table II). It is obvious that the field inferred from these data sets cannot contain the geometrical eigenmodes B_3 and B_4. These data sets contain eigenmodes B_1 and B_2 in truncated forms, as illustrated for 'SII' in Table III.

2.6. Geometrical reality of the modes B_1–B_4

The simulated data sets 'SI' and 'SII' are only illustrative. However, the following points emerge from the above results.

(i) The presence of B_1 and B_2, though in their truncated forms, in the simulated data sets 'SI' and 'SII' is due to the incorporation of approximately real butterfly diagrams in these data sets through prescription of the real annual means and standard deviations for latitudes of sunspot groups within each wing.

(ii) The absence of the 'higher degree' oscillations B_3 and B_4 in SI, and even in the more realistic simulation SII, illustrates the fact that these two oscillations will not be present in simulated data sets in which the 'distribution of sunspot activity *within* the wings of the butterflies is totally random.

We conclude that the distribution of the real sunspot activity even *within the wings* of the butterflies is *not random*. At least down to scales $l = 29$, it is defined *systematically* by superposition of the stationary and approximately stationary SHF modes of the inferred field.

From the foregoing discussion it follows that the coherent oscillations B_1, B_2, B_3, and B_4 are geometrically significant.

3. Physical Reality of the Coherent Oscillation Modes

In this section we see how the observed global latitude-time behaviours of the Sun's various 'magnetic' features, considered as measures of $B(\theta, t)$, can be reproduced by superposition of B_1, B_2, B_3, and B_4 not only in the sunspot or 'low' ($\lesssim 30°$) latitudes but also in the 'medium' (30°–75°) and the 'high' ($\gtrsim 75°$) latitudes.

3.1. The latitude distribution of B_1: confinement to low latitudes and presence of polar side-lobes

In Figure 1 we show the latitude dependence of $|B_1(\theta, t)|$ as given by all the terms in the expression

$$\sum_{l=1}^{11} a_l P_l(\mu)$$

of the dominant geometrical eigenmode $B_1(\theta, t)$. For comparison we also illustrate the latitude dependence of $|B_1(\theta, t)|$ as given by the two most dominant terms $l = 5, 7$ and the four most dominant terms $l = 3, 5, 7, 9$.

It is clear that the whole combination $l = 1$–11 is necessary and sufficient for the magnetic flux $B_1(\theta, t)$ to be confined within the latitude zone $\pm 30°$.

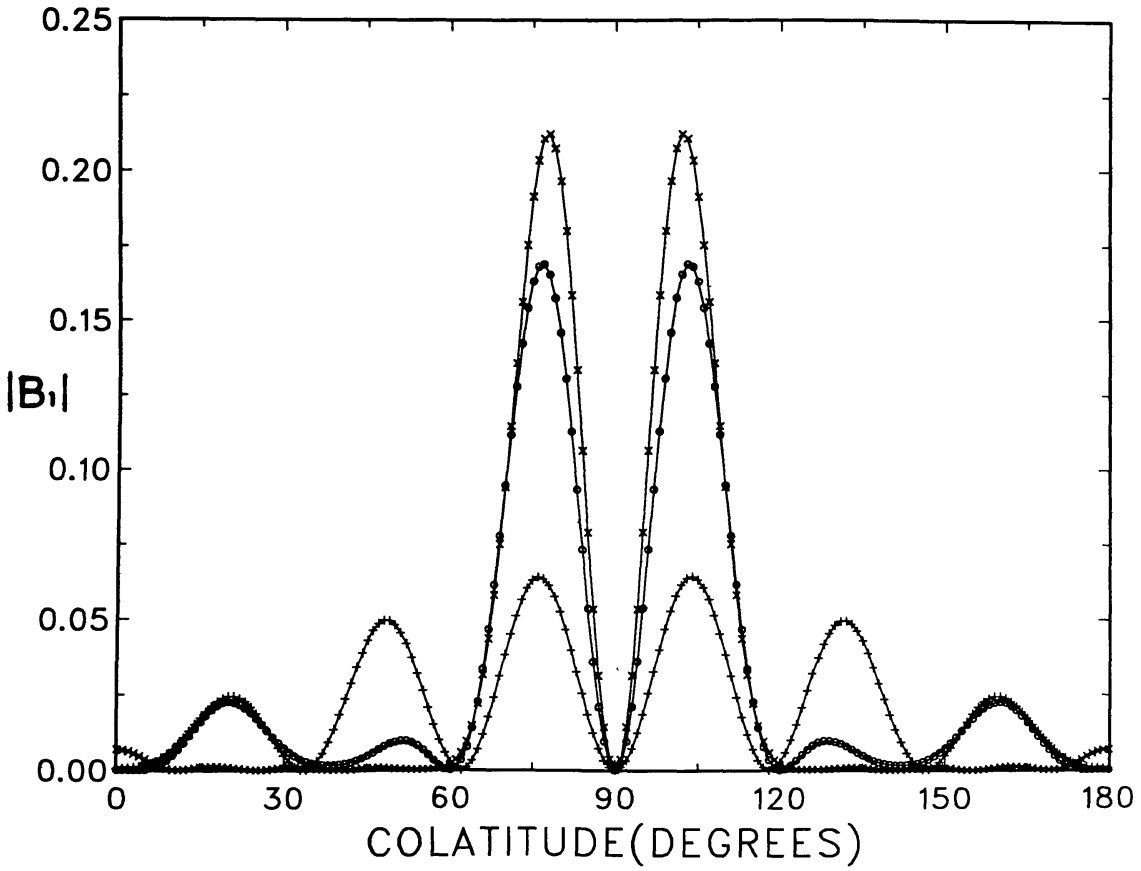

Fig. 1. Plot of $|B_1(\theta, t)|$, as a function of θ, as given by summations over terms $l = 1$ to 11 (–×–×–), $l = 3$ to 9 (–●–●–) and $l = 5, 7$ (–+–+–) in the expression for B_1 (cf. Equation (1)).

This confinement is necessarily associated with (i) existence of low side lobes up to 60° and (ii) 'moderate' 'end-lobes' near the poles.

However, it is obvious that the oscillation B_1 or any similar oscillation taken *alone* cannot yield a butterfly diagram. For, in a single coherent mode the form of the latitudinal distribution remains the same all the time, and therefore cannot give any shift of the mean latitude with time.

3.2. The latitude-time distribution of $B(\theta, t)$ given by $(B_1 + B_2)$: butterfly diagrams and the field in high latitudes

In Figure 2 we plot $B(\theta, t)$ as given by

$$B(\theta, t) = B_1(\theta, t) + B_2(\theta, t) .$$

In latitudes $\lesssim 30°$, this figure produces a butterfly diagram. To some extent this is expected since B_1 and B_2 are obtained from the dominent SHF modes in $B(\theta, t)$ which is defined as $\pm p(\theta, t)$ and $p(\theta, t)$ has the form of the butterfly diagrams. However, it is important to note that the butterfly diagram in Figure 2 is *more realistic* than the one obtained by superposing the dominent SHF modes of *even* degrees and '11 yr' periodicity in $p(\theta, t)$ *itself* (e.g., Figure 4(a) in Gokhale and Javaraiah, 1990), in the following respects:

(i) the shape and the extent of the wings is more realistic,

(ii) the overlaps between the successive sunspot cycles near the sunspot minima are present and are of the right order (viz, ~ 3 yr).

In addition, Figure 2 shows *moderate* flux concentrations in the high latitudes, which may be responsible for the polar facular activity and which like this activity, reach maxima near the 'sunspot minima' (i.e., minima of $|B(\theta, t)|$ in the low latitudes), and *vice versa* (Makarov and Sivaraman, 1989).

Further, these high latitude field concentrations, considered collectively in latitudes above 70°, change signs around the 'sunspot maxima', i.e., at about the same time as (and also in the same sense as) the observed polar fields do.

Thus the SHF modes in the inferred magnetic field '$B_{\text{inf}}(\theta, t)$' give a more realistic and more *global* description of the solar cycle phenomenon than that given by the dominent modes in the 'sunspot occurrence probability' though 'B_{inf}' has been defined in terms of 'p', and the data for 'p' comes only from the low latitudes.

3.3. The latitude time distribution of $(B_1 + B_2 + B_3)$: migration of neutral lines

In Figure 2, the 'magnetic neutral lines' do not seem to migrate up to the poles as seen in the analysis of Hα spectroheliograms by Makarov and Sivaraman (1989). Instead, in the polar regions, the migrations are away from the poles.

In Figure 3 we give the latitude time diagram given by

$$B(\theta, t) = B_1(\theta, t) + B_2(\theta, t) + B_3(\theta, t) .$$

This combination gives all the afore-mentioned properties of the $\theta - t$ distribution of

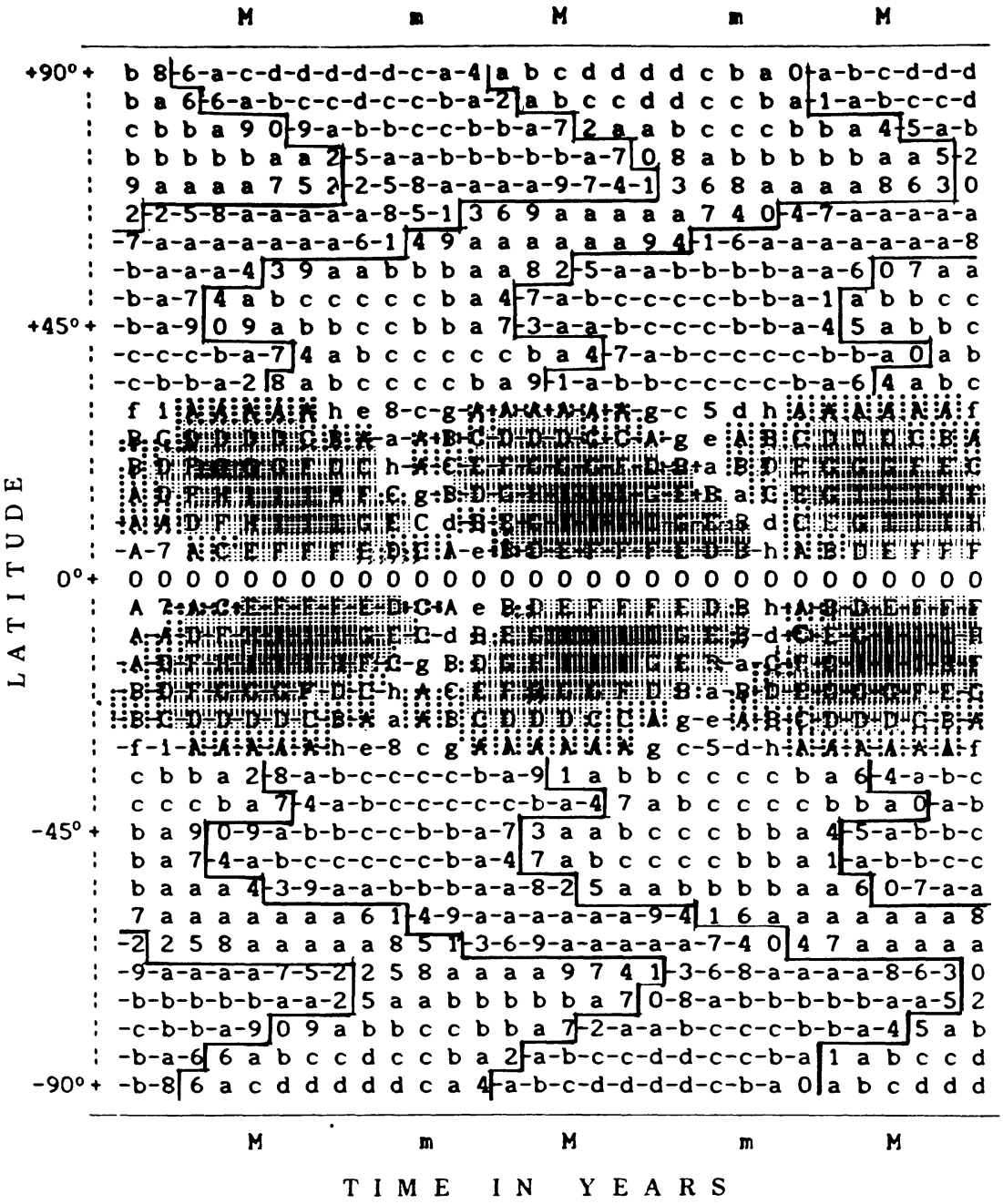

Fig. 2. Plot of $B = (B_1 + B_2)$, in arbitrary units, as a function of latitude and time (with an arbitrarily chosen zero epoch). Values with $|B| < 1$, $1 \leq |B| < 2$, $2 \leq |B| \leq 3$, ..., $9 \leq |B| < 10$, are represented by numbers 0, 1, 2, ..., 9, respectively. Similarly values with $10 \leq |B| < 20$, $20 \leq |B| < 30$, ..., $90 \leq |B| < 100$ are shown by letters a, b, c, ..., i, and those satisfying $100 \leq |B| < 200$, $200 \leq |B| < 300$, etc., are shown by letters A, B, ..., I, respectively. Years of 'solar minima' are determined as minima of $\int |B| \, d\mu$ and are denoted by 'm'. Years of expected 'maxima' ('M') are defined by $M = m + 5$. 'Neutral lines' have been drawn and the levels at and above A, D, G, and I are shaded successively darker.

$|B_1 + B_2|$ which agree with the observed global behaviour of the solar magnetic field. In addition, this also produces migrations of 'magnetic' neutral lines from the middle latitudes to poles in a way similar to that deduced by Makarov and Sivaraman. To

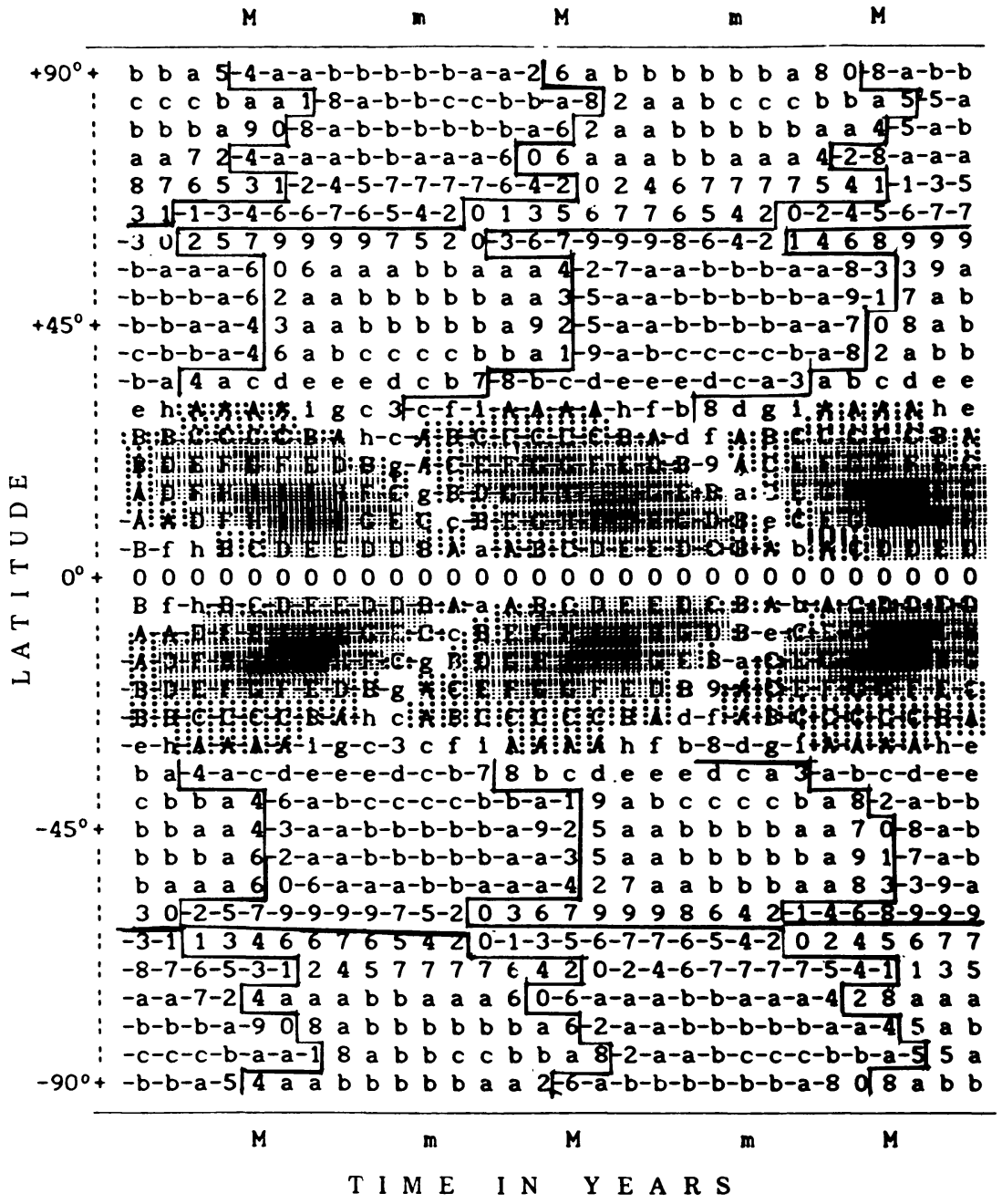

Fig. 3. Plot of $B = (B_1 + B_2 + B_3)$, in arbitrary units, as a function of latitude and time (with an arbitrary chosen zero epoch). Notations are same as in Figure 2.

migrate from $\sim 35°$ to poles these neutral lines take 15 yr, i.e., same as the real neutral lines.

3.4. The latitude-time distribution of $|B_1 + B_2 + B_3 + B_4|$

In Figure 4 we show the $\theta - t$ diagram given by

$$B(\theta, t) = B_1(\theta, t) + B_2(\theta, t) + B_3(\theta, t) + B_4(\theta, t) .$$

This figure keeps all the 'good' properties of the $\theta - t$ distribution of Figure 3. In

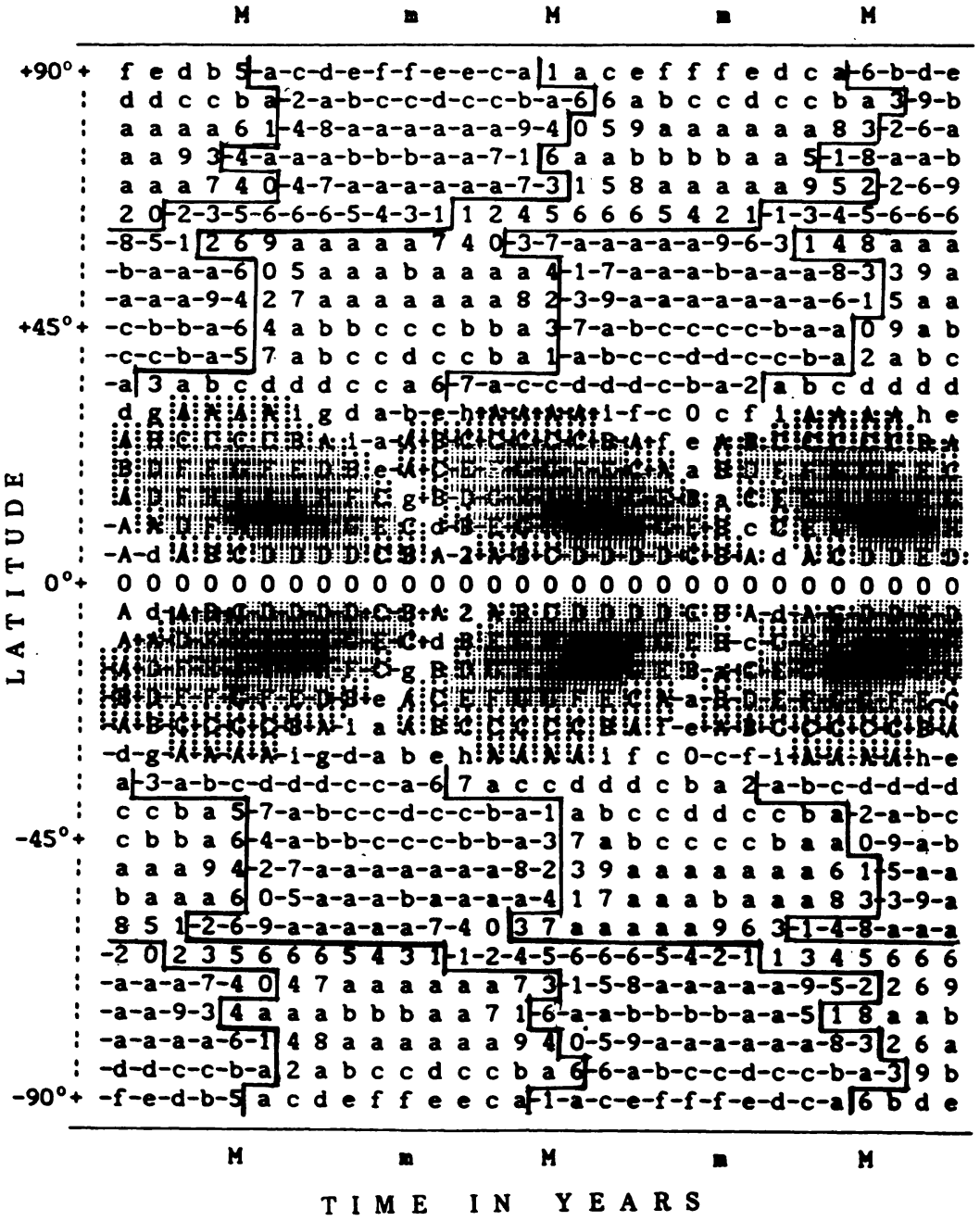

Fig. 4. Plot of $B = (B_1 + B_2 + B_3 + B_4)$, in arbitrary units, as a function of latitude and time (with an arbitrary chosen zero epoch). Notations are the same as in Figure 2.

addition, it yields, in years around sunspot minima, a somewhat higher ratio of the polar field to the field in the middle latitudes. This is necessary to account for the presence, during such years, of facular activity in high latitudes without its presence in middle latitudes.

Figures 3 and 4 do not produce the detailed real trajectories of the neutral lines in the $\theta - t$ diagrams as determined by Makarov and Sivaraman (1989). However, the agreement with the observed behaviour of the neutral lines is quite satisfactory, taking into consideration: (i) the uncertainties in the amplitudes and the phases, (ii) the

uncertainties in determining the global neutral lines using the Hα spectroheliograms, and (iii) the omission of the 'non-stationary' and the higher harmonic SHF modes as well as of the small-amplitude even degree modes which are also actually present in the inferred magnetic field.

Thus, all the four eigenmodes B_1 through B_4 are necessary and sufficient to produce a fairly satisfactory 'cleaned image model' of the observed latitude-time behaviour of the Sun's real magnetic field.

4. Comparison with Results from the Magnetogram Data

The amplitude and the relative phases of the SHF modes $l = 1$–13 determined from the sunspot data are generally similar to those obtained by Stenflo (1988) from the magnetogram data during 1960–1985, which had also given a realistic synthetic butterfly diagram. However, the sunspot data have enabled us to study the variations or constancy of the relative phases over the 103 years. Moreover, there are some important differences. (1) The relative amplitude of the mode $l = 1$ is higher (and that of $l = 3$ is lower) in the fields observed at the surface than in the field inferred from the sunspot data. We attribute this difference to the fact that, on the surface, a considerable amount of magnetic flux from the 'following' polarities of the active regions spreads into the middle latitudes, thereby transferring 'SHF power' from $l = 5$ and 3 to $l = 3$ and 1, respectively.

(2) In Stenflo's synthetic butterfly diagram the synthesized 'field strength' at the high latitudes is *of the same order as* that in the low latitudes. In contrast, the field in the high latitudes in our butterfly diagrams is of the same order as (or is only sligthly stronger than) the *weak* field in the *middle* latitudes. This is because the presence of SHF modes with $l > 13$ in our synthesis provides larger degree of interference even in the higher latitudes.

5. Conclusions and Discussion

It is clear from the discussion in Sections 2–4 that the modes in the 'main power ridge' of the SHF spectrum of the Sun's magnetic field as inferred from sunspot data constitute at least four independent distinct coherent global oscillations $B_1 \ldots B_4$. Out of these B_1 and B_2 are necessary and sufficient to produce the butterfly diagrams in the $\theta - t$ distribution of activity and are in that sense known, though not in mathematical form. The oscillations B_3 and B_4, along with non-stationary modes, define the distribution of sunspot activity within the wings of the butterflies. These do not seem to have been detected in any earlier analysis of any data.

Figure 4 gives a 'cleaned-image model' of the *mean* $\theta - t$ distribution of the Sun's internal magnetic field during 1874–1976. It is not claimed that the details of the real distribution (e.g., non-axisymmetry) which are not covered by $B_1 \ldots B_4$ are all due to noise. Nor it is claimed that the amplitudes and phases of $B_1 \ldots B_4$ are absolutely constant in reality. In fact, secular variations of amplitudes and phases of all the modes

are expected as a result of nonlinear interactions, which could (in principle) lead, in the long run, to Maunder-type modulations.

It may be mentioned here that the yearly integration of $|B(\theta, t)|$ in Figure 4 over the 'sunspot' latitudes does *not* give the *asymmetry* in the '11 yr' sunspot cycle. For reproducing the asymmetry the modes in the subsidiary power ridge at $\nu = 3\nu_*$ (and perhaps also those in $\nu = 5\nu_*$, etc.) will have to be included in $B(\theta, t)$.

The most important result of this paper is that the combination of the four coherent oscillations is necessary and sufficient to reproduce not only the observed behaviour of the real field in the low latitudes but also its *couplings* to the behaviour in the middle and the high latitudes. (A quantitative comparison of sunspot actiivty with the facular activity in the polar regions will be useful to confirm and/or improve the knowledge of coherent global oscillations of the Sun's magnetic field.) Thus the modes $B_1 \ldots B_4$ seem to be physically real, though the physical nature of these modes remain to be identified by theoretical modelling.

The definition of the 'inferred' field, as well as the difference between the results obtained from it and from the surface fields (as in Stenflo, 1988), indicate that $B_1 \ldots B_4$ represent oscillations in the Sun's internal field (which is expected to be free from complications like buoyancy, convection, amplification, and subsequent dissipation and diffusion near and above the surface).

Regarding the physical nature of the oscillations, it may only be noted (as already pointed out in Paper I), that the parities of $B_1 \ldots B_4$ are consistent with those in torsional MHD oscillations of even north–south parity in the presence of a zero-order field of dipole-like parity, and the power peak at $l = 5, 7$ would suggest dominance of $l = 6$ in the torsion. Since B_1 contains the maximum SHF power it may be defining the geometrical form of the 'forcing' oscillation.

Theoretical modelling is absolutely necessary for (i) identifying the physical nature of the coherent oscillations, (ii) predicting the form of the spectrum of the stationary modes as well as the variations of the amplitudes and phases of the non-stationary modes, and (iii) understanding the production of surface activity at the places of adequate constructive interference among oscillations of the internal field.

Acknowledgements

We thank Dr H. Balthassar for providing the magnetic tape of the sunspot data and Mr B. A. Varghese for helping with making computer plots.

References

Gokhale, M. H. and Javaraiah, J.: 1990, *Monthly Notices Roy. Astron. Soc.* **243**, 241.
Gokhale, M. H., Javaraiah, J., and Hiremath, K. M.: 1990, in J. O. Stenflo (ed.), 'Solar Photosphere, Structure, Convection and Magnetic Fields', *IAU Symp.* **138**, 375.
Gokhale, M. H., Javaraiah, J., Kutty, K. N., and Varghese, B. A.: 1992, *Solar Phys.* **138**, 35 (Paper I).
Makarov, V. I. and Sivaraman, K. R.: 1989, *Solar Phys.* **123**, 367.
Stenflo, J. O.: 1988, *Astrophys. Space Sci.* **144**, 321.